# The Production and Potential Detection of Hexamethylenetetramine-Methanol in Space

Christopher K. Materese,[1–3] Michel Nuevo,[1,2] Scott A. Sandford,[1] Partha P. Bera,[1,2] and Timothy J. Lee[4]

## Abstract

Numerous laboratory studies of astrophysical ice analogues have shown that their exposure to ionizing radiation leads to the production of large numbers of new, more complex compounds, many of which are of astrobiological interest. We show here that the irradiation of astrophysical ice analogues containing $H_2O$, $CH_3OH$, CO, and $NH_3$ yields quantities of hexamethylenetetramine-methanol (hereafter HMT-methanol; $C_7N_4H_{14}O$) that are easily detectible in the resulting organic residues. This molecule differs from simple HMT, which is known to be abundant in similar ice photolysis residues, by the replacement of a peripheral H atom with a $CH_2OH$ group. As with HMT, HMT-methanol is likely to be an amino acid precursor. HMT has tetrahedral ($T_d$) symmetry, whereas HMT-methanol has $C_1$ symmetry. We report the computed expected infrared spectra for HMT and HMT-methanol obtained using *ab initio* quantum chemistry methods and show that there is a good match between the observed and computed spectra for regular HMT. Since HMT-methanol lacks the high symmetry of HMT, it produces rotational transitions that could be observed at longer wavelengths, although establishing the exact positions of these transitions may be challenging. It is likely that HMT-methanol represents an abundant member of a larger family of functionalized HMT molecules that may be present in cold astrophysical environments. Key Words: Hexamethylenetetramine derivative—Mass spectrometry—Ice radiation chemistry. Astrobiology 20, 601–616.

## 1. Introduction

**T**HE ICES SEEN in interstellar molecular clouds are dominated by a modest number of simple molecules. $H_2O$ is generally the dominant ice component along most lines of sight, but additional common species include other simple molecules such as $CH_3OH$, $H_2CO$, $NH_3$, CO, $CO_2$, and $CH_4$ (d'Hendecourt *et al.*, 1996; Whittet *et al.*, 1996; Lacy *et al.*, 1998; Gibb *et al.*, 2000, 2004; Dartois, 2005; Boogert *et al.*, 2015). Polycyclic aromatic hydrocarbons (PAHs) and related compounds are also likely to be present (Smith *et al.*, 1989; Sellgren *et al.*, 1995; Brooke *et al.*, 1999; Bregman *et al.*, 2000; Chiar *et al.*, 2000).

Numerous laboratory studies of ice analogues containing different mixtures of these compounds have demonstrated that exposure to ionizing radiation in the form of high-energy photons or cosmic rays results in the production of numerous ions and radicals within the ices that can then recombine as the ice warms to form a wide variety of new molecular species. Many of these products are considerably more complex than those seen in the gas phase of dense clouds (Dworkin *et al.*, 2004). Some of these species are of considerable astrobiological interest and include: (1) amino acids (the building blocks of proteins) (Bernstein *et al.*, 2002a; Muñoz Caro *et al.*, 2002; Nuevo *et al.*, 2007, 2008); (2) amphiphiles (major constituents of membranes) (Dworkin *et al.*, 2001); (3) sugars and related compounds (the building blocks of carbohydrates) (Nuevo *et al.*, 2015, 2018; Meinert *et al.*, 2016); (4) quinones (molecules that play multiple roles in modern biochemistry) (Bernstein *et al.*, 1999, 2001, 2002b, 2003; Ashbourn *et al.*, 2007); (5) nucleobases (the building blocks of RNA and DNA) (Nuevo *et al.*, 2009, 2012, 2014; Materese *et al.*, 2013, 2017, 2018; Sandford *et al.*, 2015); and (6) a host of other organic compounds such as hexamethylenetetramine, ethers, urea, and hydantoin (Bernstein *et al.*, 1995, 1999; Nuevo *et al.*, 2010; de Marcellus *et al.*, 2011).

This chemistry is remarkably ''robust'' in the sense that the types of organic materials that are produced are somewhat insensitive to many of the conditions of radiation

---

[1]NASA Ames Research Center, MS 245-6, Moffett Field, California 94035.
[2]BAER Institute, NASA Research Park, MS 18-4, Moffett Field, California 94035.
[3]NASA Goddard Space Flight Center, Code 691, Greenbelt, Maryland 20771.
[4]NASA Ames Research Center, MS 245-3, Moffett Field, California 94035.

processing and warm-up. For example, the temperature of the ice during irradiation is relatively unimportant; the ice simply needs to be cold enough that the starting materials and intermediates under consideration remain condensed during irradiation. In many laboratory astrophysical ice analogues dominated by $H_2O$, the ice irradiation processes typically yield similar products over the entire 10–150 K temperature range over which the $H_2O$ ice is stable (Bernstein *et al.*, 1995). This chemistry is similarly largely insensitive to the source of the ionization (Bernstein *et al.*, 1999, 2003; Gerakines *et al.*, 2000, 2001, 2004). Finally, the basic suite of products is relatively insensitive to the composition of the ices themselves provided the ices contain sources of C, H, O, and N that can be dissociated by the incident radiation, although relative and total abundances of the products may vary (Muñoz Caro *et al.*, 2002; Bernstein *et al.*, 2002a; Elsila *et al.*, 2007; Nuevo *et al.*, 2007, 2008).

One of the first complex molecules uniquely identified in the residues produced when astrophysical ice analogues were irradiated in the laboratory was hexamethylenetetramine (Bernstein *et al.*, 1995) (also called methenamine, hexamine, aminoform, urotropin, and a host of other names, but hereafter simply referred to as HMT) (Briggs *et al.*, 1992; Bernstein *et al.*, 1995). This molecule is one of the most abundant individual molecular products formed when ices containing C, H, O, and N are irradiated (Bernstein *et al.*, 1995; Cottin *et al.*, 2001; Muñoz Caro and Schutte, 2003; Oba *et al.*, 2017).

In typical experiments, the column densities of HMT can be expected to be slightly more than 1% of the original ice's total column density and its spectral features show up clearly in the infrared (IR) spectra of bulk ice irradiation residues (Bernstein *et al.*, 1995; Muñoz Caro and Schutte, 2003).

Since only about 5% of the original ice's column density typically ends up in refractory residues, this suggests HMT abundance on the order of tens of percent in the residues.

HMT is highly soluble in water and polar organic solvents and has a cage-like structure similar to adamantane with four "corners" consisting of nitrogen atoms and "edges" consisting of methylene (–$CH_2$–) bridges (Fig. 1). Finally, the degradation products of HMT include amino acids (Wolman *et al.*, 1971), a variety of *N*-heterocycles (Vinogradoff *et al.*, 2018), and a host of other organics such as nitriles (Bernstein *et al.*, 1994, 1995; Cottin *et al.*, 2002), which makes HMT a molecule of considerable astrobiological interest.

Over many years, we have conducted numerous experiments involving the irradiation of ice mixtures containing three key components, $H_2O$, $CH_3OH$, and $NH_3$, occasionally mixed with other components (*e.g.*, CO, $CH_4$, $CO_2$). In these experiments, we detected the presence of an intense unidentified peak in the chromatograms of residues analyzed by gas chromatography coupled with mass spectrometry (GC-MS) (Fig. 2). The sharpness of the unknown peak and lack of any significant shoulders suggested that only one peak was present at this retention time, implying that this peak was resulting from the presence of a single compound rather than the contributions of several compounds that were coeluting. In addition, no other peaks in the chromatograms had a similar mass spectrum, implying that there were no alternative isomers of this molecule. Control experiments demonstrated that it was not made when ices were deposited and warmed without irradiation nor was it made when we irradiated and warmed a blank cold finger on which no ices had been deposited.

The ubiquity of this peak in the GC-MS chromatograms of the residues of irradiated mixed molecular ices containing
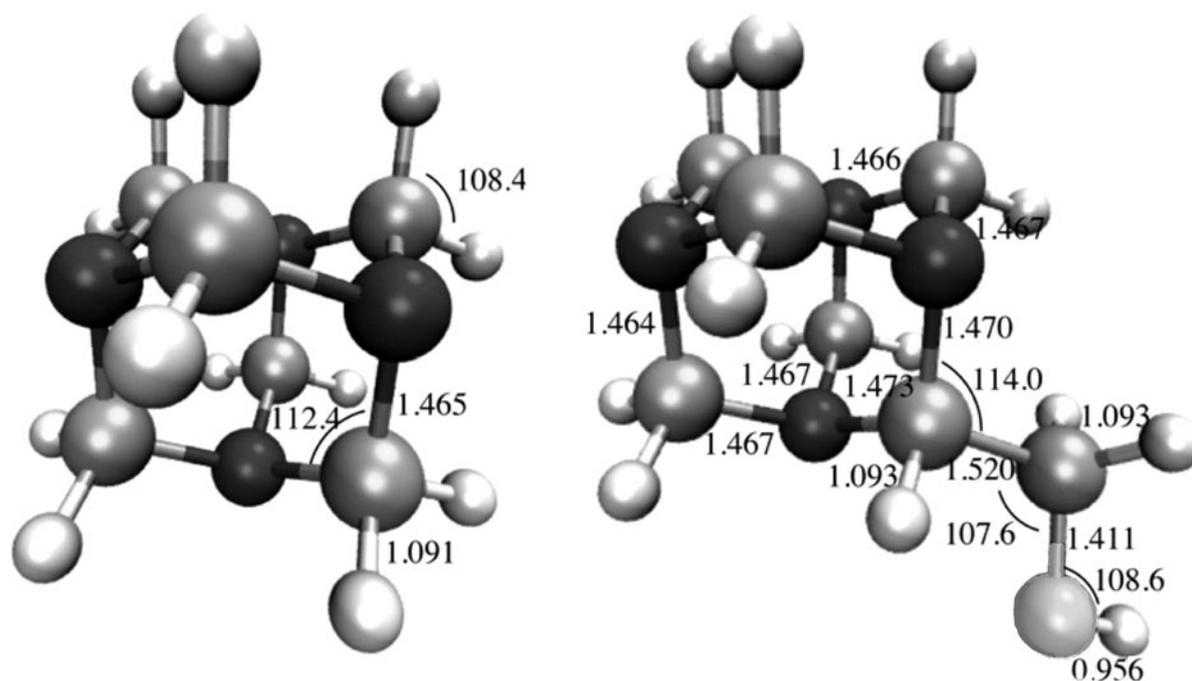


**FIG. 1.** The structural parameters computed for HMT (left) and HMT-methanol (right) using the ωB97X-D/cc-pVTZ method. Bond lengths are in Å, and bond angles are in degrees. cc-pVTZ, correlation-consistent polarized triple-zeta; HMT, hexamethylenetetramine.
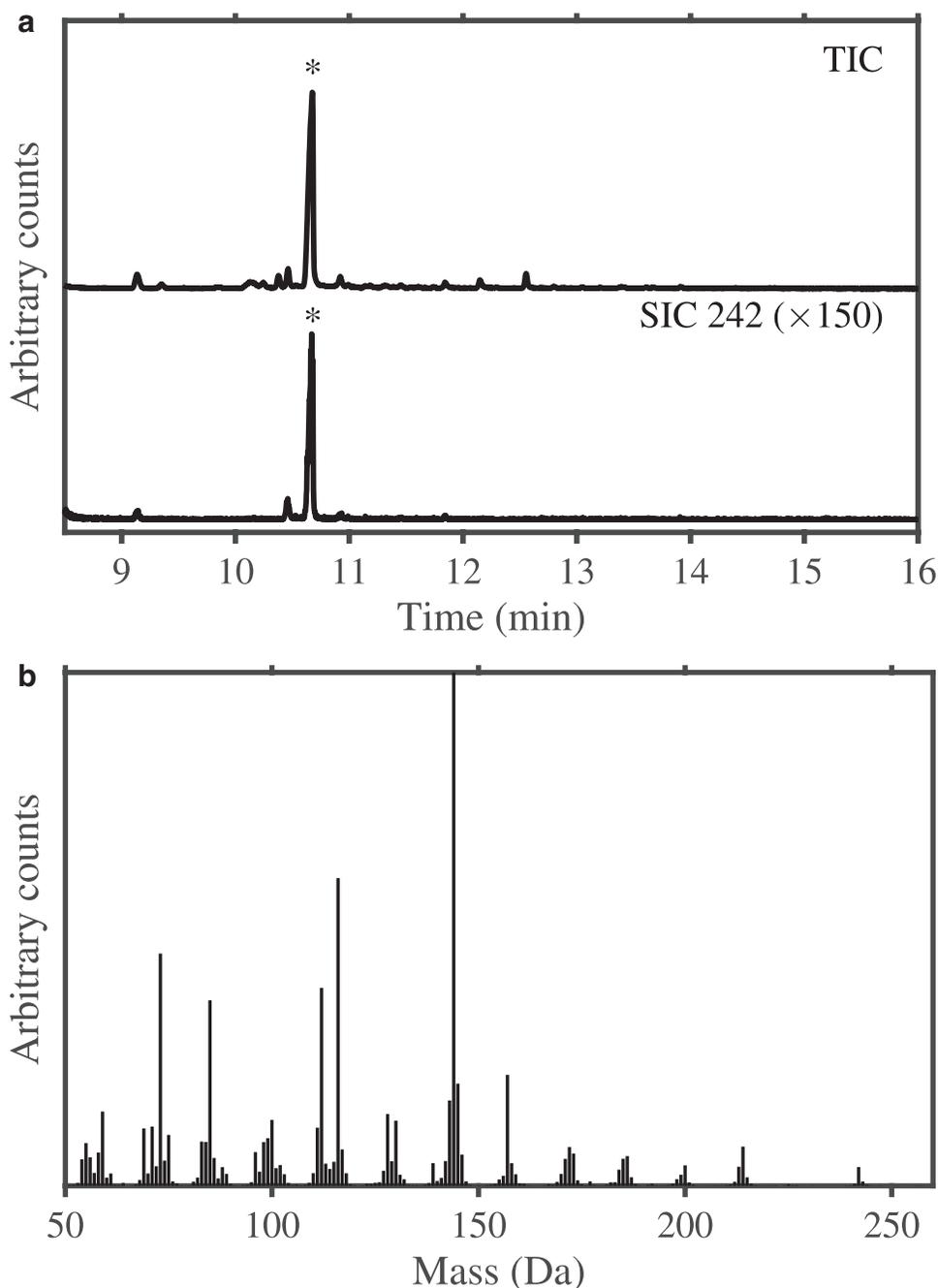
**FIG. 2.** **(a)** TIC (top trace) and SIC for $m/z = 242$ Da (*i.e.*, the molecular mass of HMT-methanol; bottom trace) of a residue produced from the UV-irradiated $H_2O$:$CH_3OH$:$CO_2$:$CO$:$NH_3$ (20:10:5:2:2) ice mixture. The most prominent peak, eluting at $\sim 10.7$ min and marked with an asterisk in the chromatograms, is associated with a mass of 242 Da and is by far the most intense in the chromatograms. **(b)** Mass spectrum associated with the 242 Da peak. Both the mass of the unknown compound and its mass spectrum indicate that it is a far more complex molecule than any of the components in the starting ice. SIC, single-ion chromatogram; TIC, total ion chromatogram; UV, ultraviolet.

$H_2O$, $CH_3OH$, and $NH_3$, its relative intensity compared with other peaks, and the apparent lack of isomers all pointed to this being a potentially interesting compound. Unfortunately, in the absence of any additional information, it was not possible to identify this product molecule.

However, we have recently carried out experiment in which the starting ice components were individually replaced with isotopic variants in which $^{12}C$, $^{14}N$, or $^{16}O$ was replaced

with $^{13}C$, $^{15}N$, or $^{18}O$, respectively (Materese *et al.*, 2018), and the resulting peak shifts in the mass spectra of the product have allowed us to identify this new product molecule as HMT-methanol, a variant of HMT where one of its peripheral H atoms is replaced with a $CH_2OH$ group. Below, we describe how these data led to this identification, and we discuss the implications of the production of this molecule and describe how it might be detected in space.

## 2. Experimental Procedures and Results

The data that ultimately allowed us to identify the source of the unknown peak (elution time of 10.7 min) shown in Fig. 2 were collected during a recent study of the formation of the purine-based nucleobases in interstellar ice analogues (Materese *et al.*, 2018). As part of that work, we carried out a series of experiments in which we individually replaced specific elements in the starting ices with heavier isotopes, that is, replaced $^{12}$C, $^{14}$N, or $^{16}$O with $^{13}$C, $^{15}$N, or $^{18}$O, respectively, to assist with identifying reaction pathways. In addition to peaks associated with purine-related products, the non-isotopically labeled GC-MS data from these experiments showed a strong peak that was associated with the same parent molecule of mass 242 Da for the $N,O$-bis(trimethylsilyl)trifluoroacetamide (BSTFA)-derivatized compound shown in Fig. 2 for non-purine containing ices. This allowed us to then examine how the mass spectrum of the unknown mass 242 Da product shifted with isotopic substitution.

We note that the absence or presence of purine in the starting ice mixtures *does not affect* this peak in the chromatograms. Indeed, the unique mass shifts seen in the isotopically labeled samples make it clear that the unknown species is created without the incorporation of any atoms from the purine (*e.g.*, if $^{13}$C-labeled CH$_3$OH was used in an ice with $^{12}$C-purine, the peak at 10.7 was $^{13}$C labeled, not $^{12}$C, the same followed for $^{15}$N-labeled NH$_3$ and $^{14}$N-labeled purine). Thus, the presence of purine plays *no essential role* in the formation of the peak eluting at ∼10.7 min. As an additional note, because the data aggregated for this work were originally collected for other purposes, they do not share exactly identical compositions (*e.g.*, there are differences in the relative abundances of H$_2$O, CH$_3$OH, NH$_3$, CO$_2$, and CO present as minor starting components of some samples such as the one shown in Fig. 1, and small amounts of purine are present as a starting component in the remaining samples). These differences, however, are inconsequential to the analysis of this peak.

All experiments described in this work involve the preparation of gas mixtures in glass bulbs attached to a vacuum manifold (background pressure ∼$5 \times 10^{-6}$ mbar). The composition of each mixture was established by measuring the partial pressures of the individual mixed gases (accurate to ∼0.05 mbar). Data shown in Fig. 2 came from ices mixtures produced from gases consisting of H$_2$O:CH$_3$OH:CO$_2$:CO:NH$_3$, with relative abundances of 20:10:5:2:2. The isotopic data discussed in this article were collected from the experiments previously published in the work of Materese *et al.* (2018). In these experiments, isotopically normal purine mixed with isotopically labeled H$_2$O:$^{13}$CH$_3$OH:NH$_3$:$^{13}$CH$_4$, H$_2$O:CH$_3$OH:$^{15}$NH$_3$:CH$_4$, and H$_2$$^{18}$O:CH$_3$$^{18}$OH:NH$_3$:CH$_4$ ice mixtures (see Materese *et al.*, 2018, for additional details). The following compounds were used in this work: H$_2$O (liquid; purified to 18.2 MΩ cm by a Millipore Direct-Q UV 3 device, and freeze-pump-thawed three times to remove excess dissolved gases), CH$_3$OH (liquid; Aldrich HPLC grade, 99.9% purity, freeze-pump-thawed three times), NH$_3$ (gas; Matheson, anhydrous, 99.99%), CH$_4$ (gas; Matheson Tri-Gas, Research purity, 99.999%), CO (gas; Scott Specialty Gases, CP grade, 99.99% purity), CO$_2$ (gas; Matheson, bone dry 99.8%), H$_2$$^{18}$O (liquid; Cambridge Isotope Laboratory, 97% $^{18}$O, freeze-pump-thawed three times), $^{13}$CH$_3$OH (liquid; Cambridge Isotope Laboratories, Inc.,

99.9% $^{13}$C), $^{15}$NH$_3$ (gas; Cambridge Isotope Laboratory, 98% $^{15}$N), and $^{13}$CH$_4$ (gas; Cambridge Isotope Laboratories, 99% $^{13}$C). Gas mixtures from these bulbs were deposited onto an aluminum foil substrate attached to a cryo-cooled (∼20 K) Raman head in a vacuum chamber (cold operating pressure of $2 \times 10^{-8}$ torr). During the deposition, mixtures were simultaneously irradiated with ultraviolet (UV) photons from a microwave-powered H$_2$ lamp. This lamp was chosen to model the radiation of stars and protostars and emits primarily Lyman-α photons (121.6 nm) in addition to a continuum centered at 160 nm, with an approximate total flux of ∼$10^{15}$ photons cm$^{-2}$ s$^{-1}$ (Warnek, 1962; Chen *et al.*, 2014). The deposition and irradiation of samples lasted between 44 and 48 h with total photon doses that were equivalent to about ∼$10^5$ years in the diffuse interstellar medium (ISM) or more than $10^8$ years in the dense ISM (Mathis *et al.*, 1983; Prasad and Tarafdar, 1983; Shen *et al.*, 2004).

At the conclusion of the deposition and irradiation, samples were gradually warmed to room temperature and the remaining residues removed from the vacuum system for analysis. Refractory materials remaining on the substrate at room temperature (hereafter referred to as residues) were recovered from the foils by using dimethylformamide, transferred to prebaked vials (500°C) and derivatized with BSTFA with 1% trimethylchlorosilane (Restek). Derivatization of the samples with BSTFA resulted in the addition of one trimethylsilyl (TMS) group (Si(CH$_3$)$_3$) to each labile hydrogen atom. Sample analysis was conducted with a Thermo Trace gas chromatograph equipped with an Agilent DB-17HT column (length: 30 m, inner diameter: 0.25 mm, film thickness: 0.15 μm), coupled to a DSQ II mass spectrometer. Samples (1 μL) were injected with an injector temperature of 250°C into a helium (carrier gas; Madco, ultrapure research grade, 99.99% purity) flow of 1.3 mL min$^{-1}$. At the start of the analysis, the column temperature was held at 100°C for 2 min and was then increased by 10°C min$^{-1}$ to a final temperature of 300°C, where it was held for 5 min. Masses were recorded between 50 and 550 Da. Chromatographic and mass spectral data were analyzed with Xcalibur™ software (Thermo Finnigan).

In the first isotope-labeling experiments, both $^{13}$C-labeled CH$_3$OH and $^{13}$C-labeled CH$_4$ were used as carbon sources in the starting ice mixtures, and this resulted in shifts in the masses of fragments seen in the mass spectra (Fig. 3 and Table 1). The $^{13}$C-labeled mass spectrum shows evidence that the $^{13}$C is present in all the molecular fragments detected by the mass spectrometer as evidenced by a shift in their mass from their standard positions. Carbon atoms associated with the derivatization tag (TMS) that is added to the residues after irradiation as part of the GC-MS analysis protocol do not contribute any additional shift. The mass of the parent peak for this $^{13}$C-labeled variant of the molecule was determined to be 249 Da, compared with 242 Da for the nonlabeled variant, implying that the product possesses seven carbon atoms (Fig. 3 and Table 1). Similar labeling experiments were repeated independently by using either $^{15}$N-labeled NH$_3$ or $^{18}$O-labeled H$_2$O and CH$_3$OH. These experiments demonstrated that the unidentified molecule possesses four nitrogen atoms and one oxygen atom (Fig. 3 and Table 1). Finally, since the derivatization agent used adds 72 Da to the mass of the molecule each time it is derivatized, and the molecular mass of the derivatized compound is consistent with only one
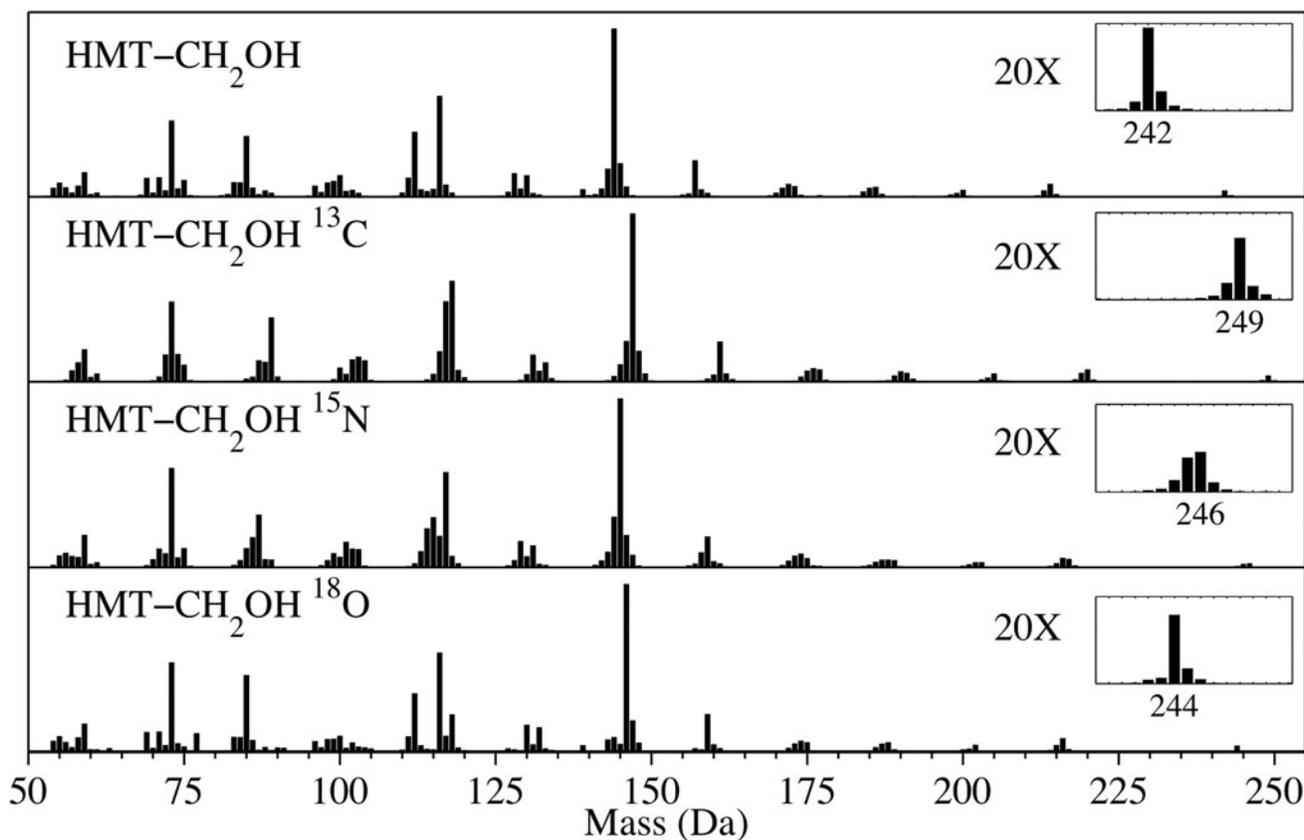
**FIG. 3.** Mass spectra of the normal, $^{13}C$, $^{15}N$, and $^{18}O$ isotopic variants (from top to bottom) of the peaks eluting at $\sim 10.7$ min observed in the GC-MS chromatograms of residues derivatized with BSTFA and assigned to HMT-methanol ($C_7H_{14}N_4O$). BSTFA, *N,O*-bis(trimethylsilyl)trifluoroacetamide; GC-MS, gas chromatography coupled with mass spectrometry.

derivatization tag attached to the molecule, this leaves 14 Da of mass unaccounted for. As hydrogen is the only other element in the ice mixture aside from C, N, and O, this implies that the empirical formula of the unidentified product molecule is $C_7H_{14}N_4O$.

The compound responsible for the intense 242 Da peak in the chromatograms is particularly interesting because, despite the large number of ways to potentially construct a molecule with an empirical formula of $C_7H_{14}N_4O$, only one isomer was observed. Importantly, we did not observe smaller precursors

TABLE 1. SUGGESTED IDENTIFICATION OF MAJOR MASS FRAGMENTS DETECTED IN THE 10.7 MIN PEAK (242 DA PARENT)

| *Mass fragments* | | | | | |
|---|---|---|---|---|---|
| *No label (Da)* | $^{13}C$ *label (Da)* | $^{15}N$ *label (Da)* | $^{18}O$ *label (Da)* | *Partial formula* | *Suggested identification* |
| 85 | 89 | 87 | 85 | $C_4N_2$ | $C_4N_2H_9$ |
| 100 | 104 | 103 | 100 | $C_4N_3$ | $C_4N_3H_{10}$ |
| 112 | 117 | 115 | 112 | $C_5N_3$ | $C_5N_3H_{10}$ |
| 116 | 118 | 117 | 116 | $C_2N$ | Unknown |
| 128 | 131 | 129 | 130 | $C_3NO$ | $C_3NOH_4+Si(CH_3)_2$ |
| 130 | 133 | 131 | 132 | $C_3NO$ | $C_3NOH_6+Si(CH_3)_2$ |
| 144 | 147 | 145 | 146 | $C_3NO$ | $C_3NOH_5+Si(CH_3)_3$ |
| 157 | 161 | 159 | 159 | $C_4N_2O$ | $C_4N_2OH_7+Si(CH_3)_2$ |
| 172 | 176 | 174 | 174 | $C_4N_2O$ | $C_4N_2OH_7+Si(CH_3)_3$ |
| 186 | 191 | 189 | 188 | $C_5N_3O$ | $C_5N_3OH_{10}+Si(CH_3)_2$ |
| 200 | 205 | 203 | 202 | $C_5N_3O$ | $C_5N_3OH_9+Si(CH_3)_3$ |
| 214 | 220 | 217 | 216 | $C_6N_3O$ | $C_6N_3OH_{11}+Si(CH_3)_3$ |
| 242 | 249 | 246 | 244 | $C_7N_4O$ | $C_7N_4OH_{13}+Si(CH_3)_3$ |

Many of these fragments are members of clusters of fragments that vary based on the number of hydrogen atoms contained. Additional fragments shown in the mass spectrum (*e.g.*, 73 Da) are associated with the derivatization agent alone.
HMT, hexamethylenetetramine.

in great abundance (*e.g.*, precursors with four, five, or six carbon atoms). In general, smaller precursors tend to be more abundant than larger compounds in ice irradiation experiments, unless there is something fairly uniquely stabilizing about the larger variant. Based on the empirical formula of $C_7H_{14}N_4O$, we hypothesized that HMT with an additional side group is the molecule responsible for this peak. HMT has already been shown to be an abundant photoproduct of astrophysical ice analogues (Bernstein *et al.*, 1995; Cottin *et al.*, 2001; Muñoz Caro and Schutte, 2003; Oba *et al.*, 2017), and a number of functionalized variants have also been suggested to exist, including HMT-methanol, based on mass spectrometry data obtained using both normal and [13]C- and ^{15}N-labeled starting ices (Muñoz Caro *et al.*, 2004). However, HMT itself could not be seen in the chromatograms of our residues, as it elutes during the same temporal window as the solvent in which the samples were dissolved and derivatized. Consequently, it was not possible to estimate the relative abundances of HMT-methanol and HMT by comparing the intensities of their peaks.

While the fragmentation pattern of the 242 Da peak cannot lead to a strictly unambiguous identification of the peak as HMT-methanol, all the fragments are consistent with this identification (Fig. 3 and Table 1). The number of C, N, and O atoms in each fragment was determined by comparing the fragmentation pattern of the isotopically unlabeled spectrum with the apparent corresponding peaks in each isotopically labeled spectrum. We inferred the number of hydrogen atoms and the presence and level of fragmentation of the attached TMS from the remaining mass that was unaccounted for. Note that the lowest mass recorded by our GC-MS protocol is 50 Da, so any smaller fragments were not detected. The first major fragment below the parent appears at 214 Da and is primarily consistent with the loss of $CH_2N$. Fragments at 200 and 186 Da are primarily consistent with the loss of $C_2H_4N$ and $C_2H_3N$, with the only further differences between these peaks being associated with fragmentation of the TMS derivative. Fragments at 172 and 157 Da are primarily consistent with the loss of $C_3H_6N_2$. Fragments at 144, 130, and 128 Da appear to be primarily associated with a loss of $C_4N_3H_8$, $C_4N_3H_7$, and $C_4N_3H_9$, respectively. All these fragments are consistent with what might be expected from the rupture of the HMT cage. Additional fragments at 112, 100, and 85 Da are all consistent with an HMT remnant after loss of fragments that include the methanol side group. All the previously suggested fragment identifications are based on shifts in the positions of the major mass peaks with respect to isotopic labeling. One additional fragment of interest at 139 Da may be associated with the HMT cage itself after the loss of the $CH_2O$+TMS group. Based on the isotopic labeling, it is clear that this fragment contains no oxygen, which is consistent with the aforementioned identification. However, if this identification is correct, then it is extremely difficult to unambiguously establish the number of carbon and nitrogen atoms in this fragment because the associated mass peaks would be expected to overlap with other larger fragments.

If we assume that HMT ($C_6H_{12}N_4$) serves as the structural basis for this molecule, there are three possible isomers that could yield an empirical formula of $C_7H_{14}N_4O$: HMT+$CH_2OH$ (HMT-methanol), HMT+OH+$CH_3$ (hydroxyl, methyl-HMT), or HMT+$OCH_3$ (methoxy-HMT). The HMT+$OCH_3$ variant can be quickly eliminated as a possible carrier for this peak because

this compound cannot be derivatized by the chromatographic method we used and therefore is not consistent with the observed parent mass of 242 Da. Notably, no other peaks with the same parent mass and similar fragmentation patterns were observed in our chromatograms. This suggests that of the remaining two possibilities, HMT-$CH_2OH$ is far more likely to be the source of this peak than an HMT+OH+$CH_3$ variant, because the former has no structural isomers, whereas the latter has multiple isomers involving different relative placements of the OH and $CH_3$ side groups on the HMT cage structure. Additionally, $CH_3OH$ has been shown to possess photodissociation branching ratios of $\sim 1:1:5$ for •$CH_3$/•OH, •$OCH_3$, and •$CH_2OH$ radicals, respectively (Öberg *et al.*, 2009), making •$CH_2OH$ a far more abundant reactant in our ice. Thus, $CH_2OH$ is more likely to be found as a functional group in products formed from the irradiation of $CH_3OH$ and cyclic organic compounds, as was previously observed with ices containing pyrimidine (Materese *et al.*, 2013; Nuevo *et al.*, 2014) and purine (Materese *et al.*, 2018).

Finally, we would note that while HMT-$OCH_3$ is not consistent with the parent mass at 242 Da, this does not necessarily imply that HMT-$OCH_3$ is not present in the samples. Mass filtering of our data for the mass of underivatized HMT-$OCH_3$ (170 Da) showed no peaks in the chromatograms consistent with the presence of this molecule. However, this does not preclude the possibility that this molecule was eluting outside the range of retention times we recorded.

## 3. Computational Procedures and Results

Structural and spectroscopic characteristics of HMT and HMT-methanol have been investigated by using the ωB97X-D density functional theory method (Mardirossian and Head-Gordon, 2017) along with the correlation-consistent polarized valence triple-zeta (cc-pVTZ) basis set (Dunning, 1989) that includes *spdf* functions for C, N, and O atoms, and *spd* functions for H atoms. All calculations were performed with the Q-Chem 4 quantum program package (Shao *et al.*, 2015). Structural parameters thus obtained are accurate to within $\sim 10^{-3}$ Å relative to the experimental values. The gas-phase optimized geometrical structures of HMT and HMT-methanol are presented in Fig. 1. Due to the high tetrahedral ($T_d$) symmetry of HMT, all C–N bond lengths are of equal value (1.465 Å), and all C–H bond lengths are 1.091 Å, whereas the NCN and HCH bond angles are 112.4° and 108.4°, respectively. HMT-methanol possesses $C_1$ symmetry due to the presence of the $CH_2OH$ group. The lone C–C bond length is 1.520 Å, that is, slightly elongated compared with the value of 1.512 Å for ethanol. The C–N bonds nearest to the $CH_2OH$ group are slightly elongated as well, but all are relatively close (less than 0.005 Å difference) to those in the parent HMT molecule. The C–H bond lengths are also similar to the canonical value for HMT, whereas the O–H bond length (0.956 Å) is similar to the value in methanol (0.956 Å). Finally, the C–O bond (1.411 Å) is slightly shorter than that of ethanol (1.431 Å) and methanol (1.427 Å). Bond length values for ethanol and methanol were taken from the Computational Chemistry Comparison and Benchmark DataBase (https://cccbdb.nist.gov/alldata2.asp?casno=74840).

The band positions of the harmonic vibrational frequencies, together with their integrated IR band intensities, are given in Table 2 for HMT and in Table 3 for HMT-

TABLE 2. HARMONIC VIBRATIONAL FREQUENCIES (CM$^{-1}$) AND INTEGRATED INFRARED BAND INTENSITIES (IN KM MOL$^{-1}$) OF HEXAMETHYLENETETRAMINE ($T_d$ SYMMETRY) COMPUTED USING THE ωB97X-D/CC-PVTZ METHOD

| Symmetry | Vibrational mode | Frequency (cm$^{-1}$)* | Band position (μm)* | Intensity (km mol$^{-1}$) |
|---|---|---|---|---|
| $A_1$ | Totally symmetric CH stretch | 3070 | 3.257 | 0 |
| $A_1$ | Totally symmetric HCH scissor | 1556 | 6.427 | 0 |
| $A_1$ | Totally symmetric bend | 1069 | 9.355 | 0 |
| $A_1$ | Totally symmetric CN stretch | 814 | 12.29 | 0 |
| $A_2$ | Antisymmetric CH rock | 1252 | 7.987 | 0 |
| E | Symmetric CH stretch | 3054 | 3.274 | 0 |
| E | HCH symmetric scissor | 1518 | 6.588 | 0 |
| E | HCH symmetric rock | 1402 | 7.133 | 0 |
| E | CN symmetric stretch | 1086 | 9.208 | 0 |
| E | CNC symmetric bend | 484 | 20.66 | 0 |
| $T_1$ | Symmetric CH stretch | 3106 | 3.220 | 0 |
| $T_1$ | HCH wag-twist | 1390 | 7.194 | 0 |
| $T_1$ | HCH twist-wag | 1377 | 7.262 | 0 |
| $T_1$ | HCH twist-rock | 1107 | 9.033 | 0 |
| $T_1$ | HCH rock | 988 | 10.12 | 0 |
| $T_1$ | HCH rock | 415 | 24.10 | 0 |
| $T_2$ | Antisymmetric CH stretch | 3111 | 3.214 | 163.8 |
| $T_2$ | Antisymmetric CH stretch | 3058 | 3.270 | 317.7 |
| $T_2$ | HCH scissor | 1532 | 6.527 | 56.4 |
| $T_2$ | HCH wag | 1441 | 6.940 | 49.2 |
| $T_2$ | CN stretch | 1299 | 7.698 | 209.7 |
| $T_2$ | Antisymmetric CN stretch | 1063 | 9.407 | 437.7 |
| $T_2$ | CN stretch | 868 | 11.52 | 48.6 |
| $T_2$ | NCN bend | 714 | 14.01 | 74.7 |
| $T_2$ | HCH rock | 545 | 18.35 | 7.2 |

The IR intensities for degenerate bands have been multiplied by the appropriate degeneracy factor.

*Actual frequencies/positions will shift to the red from these values by different amounts when anharmonicity is taken into consideration (see text for detailed discussion).

cc-pVTZ, correlation-consistent polarized triple-zeta; IR, infrared.

methanol. These values will shift if anharmonicity is taken into account, and these shifts will vary depending on the nature of the vibrational mode. For example, the average anharmonic correction for the C–H stretching modes in methane is ∼137 cm$^{-1}$ (Lee *et al.*, 1995), which corresponds to the largest anharmonic correction for any of the modes in HMT. The O–H stretch in HMT-methanol will have a slightly larger anharmonic correction as evidenced by the average anharmonic correction for the frequencies of the O–H stretches in water of ∼187 cm$^{-1}$ (Huang and Lee, 2008). From our experience, the anharmonic corrections for all the other modes will be much smaller, in the 0–30 cm$^{-1}$ range, with the possible exception of the hindered rotor motions associated with the CH$_2$OH group in HMT-methanol. These hindered rotor motions involve large-amplitude motions, and while their harmonic frequencies are relatively low, the anharmonic correction could be a substantial fraction of the harmonic frequency. Thus, most of the harmonic vibrational frequencies, with the exceptions listed above, should be within ∼20 cm$^{-1}$ of the experimental fundamental vibrational frequencies. This level of accuracy for the non-C–H stretching vibrational modes should be reliable enough to assign low-resolution spectra such as from Spitzer, ISO, or the upcoming JWST, but would not be reliable enough to assign high-resolution spectra from instruments such as TEXES (used at the IRTF) or EXES (used on SOFIA).

The computed vibrational spectra of HMT and HMT-methanol, using the harmonic vibrational frequencies and integrated IR band intensities, are shown in Fig. 4 and compared with the laboratory spectrum of HMT isolated in an Ar-matrix from the work of Bernstein *et al.* (1994). Arrows have been placed on top of several representative IR bands that show the expected shifts that would result from anharmonic corrections to the calculated spectra. While there are no experimental spectra of HMT-methanol available for comparison with these calculations, the vibrational bands associated with the HMT skeleton fall very close to the experimental HMT bands once the expected anharmonicities are taken into account, so the computed values for HMT-methanol are expected to be similarly close.

For HMT, two sets of triply degenerate C–H stretching vibrations appear with large intensities: one set at 3058 cm$^{-1}$ (3.270 μm), each with an intensity of 105.9 km mol$^{-1}$ (for a total IR intensity of 317.7 km mol$^{-1}$), and another set at 3111 cm$^{-1}$ (3.214 μm), each with an intensity of 54.6 km mol$^{-1}$ (for a total IR intensity of 163.8 km mol$^{-1}$). Taking into account anharmonicity, as discussed above, these two C–H stretch bands are in good agreement with the experimental spectrum, except that it is clear that there are more than two bands in the experimental spectrum. This is likely due to the need to include Fermi resonances, which has been found to be very important for computed anharmonic spectra of PAH molecules (Mackie *et al.*, 2015). Two sets of triply degenerate C–N stretching modes also show large intensity vibrations at 1063 cm$^{-1}$ (9.407 μm) with the strongest total intensity of 437.7 km mol$^{-1}$, and another set at 1299 cm$^{-1}$ (7.698 μm) with a total intensity of 209.7 km mol$^{-1}$. Both these C–N stretching modes are in good agreement with experimental values.

TABLE 3. HARMONIC VIBRATIONAL FREQUENCIES ($cm^{-1}$) AND INTEGRATED INFRARED BAND INTENSITIES (IN KM $MOL^{-1}$) OF HEXAMETHYLENETETRAMINE-METHANOL ($C_1$ SYMMETRY) COMPUTED USING THE ωB97X-D/cc-pVTZ METHOD

| Frequency ($cm^{-1}$) | Band position ($\mu m$) | Intensity ($km\ mol^{-1}$) | Frequency ($cm^{-1}$) | Band position ($\mu m$) | Intensity ($km\ mol^{-1}$) |
|---|---|---|---|---|---|
| 73 | 138 | 6.9 | 1275 | 7.844 | 55.9 |
| 161 | 62.0 | 2.4 | 1283 | 7.796 | 97.5 |
| 199 | 50.2 | 97.0 | 1289 | 7.756 | 20.9 |
| 259 | 38.6 | 7.8 | 1311 | 7.627 | 14.7 |
| 342 | 29.3 | 0.7 | 1336 | 7.483 | 1.3 |
| 404 | 24.8 | 0.1 | 1346 | 7.431 | 4.3 |
| 413 | 24.2 | 0.8 | 1353 | 7.394 | 0.4 |
| 445 | 22.5 | 1.8 | 1358 | 7.363 | 0.4 |
| 480 | 20.8 | 1.6 | 1362 | 7.344 | 0.9 |
| 512 | 19.5 | 7.2 | 1371 | 7.293 | 2.0 |
| 535 | 18.7 | 2.2 | 1378 | 7.260 | 0.3 |
| 543 | 18.4 | 1.3 | 1389 | 7.198 | 5.1 |
| 563 | 17.8 | 6.2 | 1410 | 7.094 | 18.7 |
| 688 | 14.5 | 33.6 | 1411 | 7.085 | 14.7 |
| 701 | 14.3 | 20.5 | 1417 | 7.059 | 17.2 |
| 710 | 14.1 | 21.5 | 1487 | 6.727 | 3.5 |
| 804 | 12.4 | 3.1 | 1495 | 6.690 | 2.9 |
| 831 | 12.0 | 6.3 | 1503 | 6.656 | 5.6 |
| 855 | 11.7 | 12.3 | 1513 | 6.609 | 15.7 |
| 882 | 11.3 | 14.7 | 1517 | 6.593 | 16.4 |
| 946 | 10.6 | 25.1 | 1537 | 6.505 | 8.6 |
| 964 | 10.4 | 2.7 | 1543 | 6.480 | 4.7 |
| 979 | 10.2 | 28.3 | 3018 | 3.313 | 33.7 |
| 1005 | 9.946 | 23.2 | 3050 | 3.279 | 30.4 |
| 1049 | 9.534 | 152.7 | 3051 | 3.277 | 18.4 |
| 1055 | 9.479 | 92.7 | 3053 | 3.276 | 45.3 |
| 1060 | 9.431 | 84.2 | 3058 | 3.270 | 64.9 |
| 1062 | 9.417 | 6.8 | 3065 | 3.263 | 67.6 |
| 1071 | 9.336 | 16.3 | 3070 | 3.258 | 53.8 |
| 1078 | 9.275 | 1.0 | 3073 | 3.254 | 29.2 |
| 1092 | 9.159 | 9.0 | 3101 | 3.225 | 8.8 |
| 1106 | 9.045 | 69.6 | 3105 | 3.221 | 33.3 |
| 1134 | 8.816 | 15.9 | 3108 | 3.218 | 41.2 |
| 1151 | 8.690 | 11.5 | 3116 | 3.209 | 16.5 |
| 1222 | 8.185 | 67.6 | 3121 | 3.204 | 45.4 |
| 1237 | 8.083 | 2.4 | 3925 | 2.548 | 43.7 |

For example, Bernstein *et al.* (1994) reported the $\nu_{22}$ C–N stretching mode vibration, the strongest peak of HMT isolated in an Ar-matrix at 22 K, to be at $1011\,cm^{-1}$ ($9.891\,\mu m$), which is within $52\,cm^{-1}$ of the calculated position. This difference in band position is due to a combination of a shift resulting from the interaction of HMT with the Ar-matrix on the experimental side, and the absence of anharmonic corrections in the *ab initio* computed spectrum.

The second strongest band ($\nu_{21}$) measured experimentally in the Ar-matrix spectrum has a frequency of $1238\,cm^{-1}$ ($8.080\,\mu m$), that is, $61\,cm^{-1}$ lower than the value obtained from the *ab initio* computed spectra in this work, which is consistent with the shift observed for the $\nu_{22}$ C–N stretching mode. One notable difference between the experimental (Bernstein *et al.*, 1994) and the theoretical spectra (this work) is that the C–H stretching modes appear much stronger in intensity in the gas-phase calculation than in the Ar-matrix experiments, which has been observed previously for PAH molecules (Joblin *et al.*, 1994). In other words, the IR intensity of the C–H stretches is known to be smaller in matrix studies than predicted in computed spectra relative to other vibrational bands. The C–N stretching modes of the HMT-methanol are expected to display similar shifts between

the computed harmonic vibrational frequencies and the experimental fundamental vibrational frequencies as those found for HMT.

Another important difference between the vibrational modes of HMT and HMT-methanol that is evident in Tables 2 and 3 is the intensities of the bands. Due to the $T_d$ symmetry of HMT, only the triply degenerate $T_2$ vibrational modes are IR active, whereas all the other vibrational modes are IR inactive and thus have an intensity of zero.

The presence of the $CH_2OH$ side group in HMT-methanol drastically lowers the symmetry from $T_d$ to $C_1$, resulting in vibrational modes for HMT-methanol, which all have nonzero IR intensities. This symmetry breaking removes the degeneracy of the vibrational bands, and in many cases results in a number of closely spaced bands with similar intensities. It is clear from Table 3 and Fig. 4 that the $CH_2OH$ addition should be seen as a perturbation on the overall HMT vibrational spectrum, similar to the previous discussion regarding the molecular geometries. Thus, the vibrational modes that are IR inactive in the spectrum of HMT are IR active with small intensities in the spectrum of HMT-methanol, resulting in a large number of bands with very small IR intensities compared with the most intense modes. One additional item to note regarding the IR intensities of
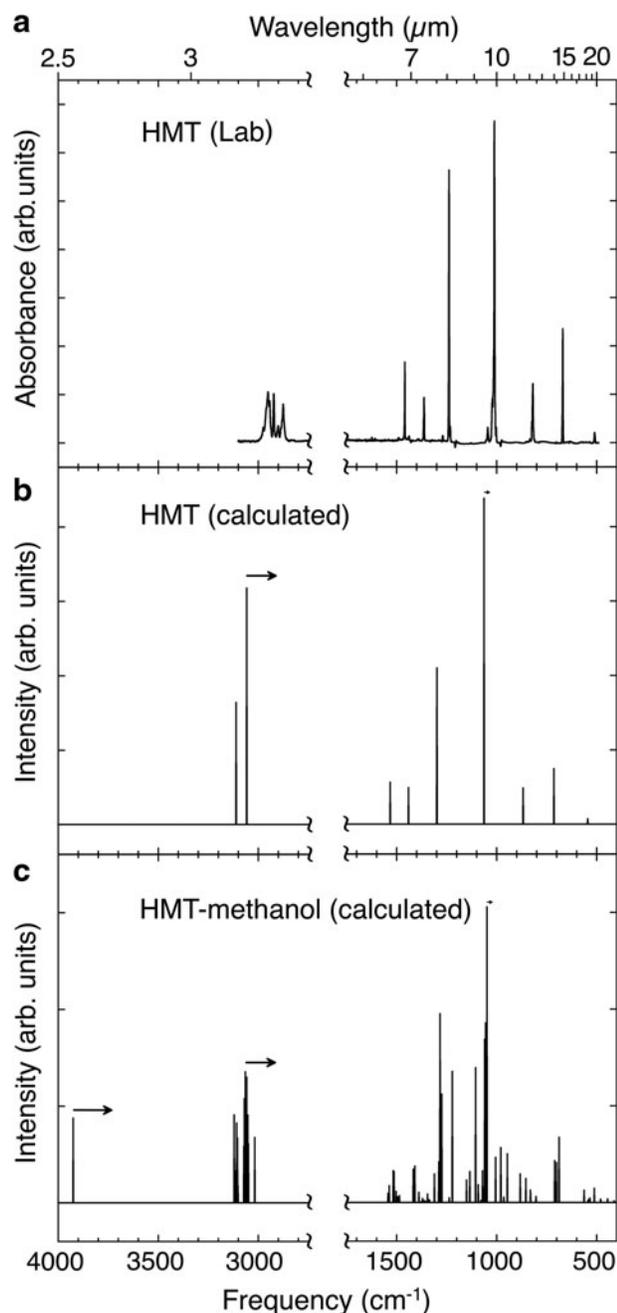
**FIG. 4.** **(a)** Experimentally measured IR spectrum of HMT isolated in an Ar-matrix (Bernstein *et al.*, 1994). This spectrum is compared with the computed harmonic vibrational spectra of **(b)** HMT and **(c)** HMT-methanol using the ωB97X-D/cc-pVTZ method. Arrows above representative IR bands near 3925, 3070, and 1045 cm$^{-1}$ (2.548, 3.257, 9.566 μm, respectively) in the computed spectra indicate the direction and magnitude of band shifts expected if anharmonicity was taken into account. IR, infrared.

HMT-methanol concerns bands with high intensities in the spectrum of HMT. Since the IR active modes of HMT are all triply degenerate, it is possible for the most part to correlate these bands in HMT with the corresponding bands in the spectrum of HMT-methanol. A good example is given by the most intense vibrational band of HMT at 1063 cm$^{-1}$ (9.407 μm), which has a computed intensity of 437.7 km mol$^{-1}$

(with the degeneracy factor included) that correlates well with the bands at 1049, 1055, and 1060 cm$^{-1}$ (9.534, 9.479, and 9.431 μm, respectively) of HMT-methanol with a combined IR intensity of 330 km mol$^{-1}$. However, such correlations are not straightforward for the C–H stretching modes for which the total IR intensity for HMT seems to be distributed across all C–H stretching bands, which is probably related to a larger number of Fermi resonances in HMT-methanol due to its lowered molecular symmetry.

The bands mentioned above at 1049, 1055, and 1060 cm$^{-1}$ are the three strongest bands of HMT-methanol and have intensities of 152.7, 92.7, and 84.2 km mol$^{-1}$, respectively. All three of these bands are associated with C–N stretching modes of the HMT cage structure. The strong C–N stretching mode of HMT-methanol at 1049 cm$^{-1}$ (9.534 μm) is largely unchanged from the corresponding single degenerate mode of HMT at 1045 cm$^{-1}$ (9.566 μm). A number of vibrational modes associated with rocking motions of $CH_2$ groups in the HMT skeleton appear near the largest peak at 1049 cm$^{-1}$ (9.534 μm) described above. Three C–H stretching modes with significant intensities that are associated with $CH_2$ groups in the HMT cage appear at 3053, 3058, and 3065 cm$^{-1}$ (3.276, 3.270, and 3.263 μm, respectively). While there are no experimental spectra of HMT-methanol available for comparison with these calculations, the bands associated with vibrational modes in the HMT skeleton fall very close to the experimental HMT vibrational bands once the expected anharmonic shifts are accounted for (see above and Fig. 4).

There are several vibrational bands that appear in the spectrum of HMT-methanol but that are absent that of HMT. These are all due to vibrations associated with the $CH_2OH$ side group in HMT-methanol. The harmonic frequency value at 1151 cm$^{-1}$ (8.690 μm) is identified as the C–C stretch in HMT-methanol, which is typical of a C–C single bond, as supported by the computed 1163 cm$^{-1}$ (8.599 μm) frequency for acetaldehyde (Simandiras *et al.*, 1988). The O–H stretching band of the $CH_2OH$ group on HMT-methanol is easily identified at 3925 cm$^{-1}$ (2.548 μm), a value typical for this mode as demonstrated by the average of the symmetric and antisymmetric frequencies for $H_2O$ at 3897 cm$^{-1}$ (2.566 μm) (Huang and Lee, 2008). The O–H bending motion of the side group is responsible for the 1106 cm$^{-1}$ (9.045 μm) band with an intensity of 69.6 km mol$^{-1}$. The high-intensity vibrational modes at 1222 and 1275 cm$^{-1}$ (8.185 and 7.844 μm, respectively) are due to two HCO bending modes of the side group, and the band at 1283 cm$^{-1}$ (7.796 μm) is due to an HOC bending mode of the side group. Finally, the strong band at 199 cm$^{-1}$ (50.2 μm) in the HMT-methanol spectrum that is not present in the spectrum of HMT is due to the HCOH dihedral angle bending mode of the $CH_2OH$ side group.

## 4. Discussion and Implications

### 4.1. Mechanism of formation of HMT-methanol

There are two general ways in which HMT-methanol might be formed during the UV irradiation and warming of astrophysical ice analogues: (1) via the formation of HMT first, followed by the substitution of a peripheral H atom of HMT with a $CH_2OH$ group; and (2) via an independent pathway similar to the one(s) that produce HMT in which a $CH_2OH$ group is added to one of the intermediate species. We discuss both possibilities below.

Some researchers have described reaction schemes for the production of HMT (Smolin and Rapoport, 1959; Bernstein *et al.*, 1995; Woon, 2001; Zeffiro *et al.*, 2016). These suggested mechanisms differ in detail but all describe reaction paths that involve formaldehyde and ammonia as starting reactants, and methyleneimine (CH$_2$=NH) (or something very similar) as a key intermediary. These molecules have all been detected in space (Cheung *et al.*, 1968; Snyder *et al.*, 1969; Godfrey *et al.*, 1973; Dickens *et al.*, 1997) and are known to form during the UV irradiation of mixed molecular ices containing CH$_3$OH and/or CO (Bernstein *et al.*, 1995; Harich *et al.*, 1999). However, all these proposed mechanisms involve only neutrals and are presumed to occur at temperatures at which energy barriers are not an issue, that is, under conditions that are not representative of low-temperature ice photochemistry.

The mechanism(s) of formation of HMT have also been studied in conditions closer to our experiments, from the irradiation of ices containing CH$_3$OH and/or CO and NH$_3$ with UV photons (Bernstein *et al.*, 1995; Cottin *et al.*, 2001; Muñoz Caro and Schutte, 2003; Muñoz Caro *et al.*, 2004; Vinogradoff *et al.*, 2013) or energetic protons (Cottin *et al.*, 2001), and/or the warm-up of ices containing H$_2$CO and NH$_3$ or H$_2$CO, formic acid, and methylamine without irradiation (Vinogradoff *et al.*, 2012). One important result of these studies is that the formation of HMT itself largely occurs via a pure thermal process during warm-up without any additional irradiation being required (Bernstein *et al.*, 1995; Muñoz Caro and Schutte, 2003; Vinogradoff *et al.*, 2011, 2012, 2013). HMT formation is clearly seen to occur at temperatures above 200 K (Bernstein *et al.*, 1995; Vinogradoff *et al.*, 2012) and continues after the samples reach room temperature (Muñoz Caro and Schutte, 2003; Vinogradoff *et al.*, 2011, 2013). This indicates that only the precursors of HMT are formed in low-temperature ices. The same is likely true for HMT-methanol.

Experience with ice photochemistry suggests that the formation of HMT and its precursors from the irradiation of ices at low temperature is unlikely to follow a simple mechanism because such processes are known to result in the production of a large number of reactive species, such as ions and radicals, which can react with each other or with neutral molecules without being limited by energy barriers. The radiation also breaks down intermediate products that can go on to participate in subsequent reactions. The net result is a stochastic process that can produce complex products following multiple different paths, many of which involve ions and/or radicals. This has been demonstrated for the production of amino acids (Elsila *et al.*, 2007) and nucleobases (Bera *et al.*, 2010, 2016) from the UV irradiation of ices, and is also likely to be true for the production of HMT and related compounds.

H$_2$O may also play an important role in the formation of HMT and its precursors, as it may help lowering the activation barriers of reactions. Indeed, the formation of HMT was shown to be more efficient when increasing the concentration of H$_2$O in the starting ices (Muñoz Caro and Schutte, 2003; Muñoz Caro *et al.*, 2004). This suggests that H$_2$O molecules may also work like catalysts in the HMT formation process, much as they do in the case of the formation of nucleobases when pyrimidine and purine are irradiated in H$_2$O-rich ices (Bera *et al.*, 2010, 2016, 2017). The role of H$_2$O as a catalyst is also supported by a theoretical study that has shown, using a conductor-like polarizable continuum model, that H$_2$O molecules help the reaction between formaldehyde and ammonia that produces methyleneimine, a key precursor to HMT (Riffet *et al.*, 2018).

Finally, we would note that the formation of HMT-methanol from the addition of a CH$_2$OH group to HMT is probably less efficient than the addition of a CH$_2$OH group to an intermediate compound. This is because, as previously discussed, the formation of the majority of HMT appears to occur during and after warming to room temperature when (1) the samples are no longer subjected to UV radiation to drive substitution, (2) most of the CH$_3$OH and H$_2$CO have sublimed away, and (3) most reactive species have already reacted. However, it is more likely that during the photo-irradiation of the ices at low temperature, CH$_2$OH groups could be added (via CH$_2$OH radicals, ions, and/or CH$_3$OH) to any intermediate species that are subsequently involved in the formation of HMT-methanol.

In short, the production of HMT from ice UV irradiation and warm-up is likely the result of multiple pathways that involve formaldehyde and methyleneimine as key intermediaries and that include both neutral and ion–molecule reactions. This is likely to be true for other HMT variants, which may form (1) through the addition of side groups to previously formed HMT during warm-up and/or at room temperature and (2) through similar but independent ''bottom-up'' pathways in which the photo-induced addition of side groups to intermediate compounds at low temperature results in the formation of a variety of HMT derivatives during warm-up, with the latter pathway likely to be dominant.

### 4.2. The search for HMT, HMT-methanol, and other HMT derivatives in space

**4.2.1. Where to search.** While the photolysis of mixed molecular ices is central to the formation of HMT and its variants, the ice matrix hinders the mobility of created reactants and limits chemical reactions to adjacent species. Thus, while reactants such as methyleneimine and formaldehyde can be formed within the ice, the multistep formation of HMT and its variants is expected to be very inefficient in low-temperature ices. The majority of HMT and its variants are instead formed when the ice is warmed, volatile species sublime, and reactants become more mobile. As a result, the IR spectral features of HMT are extremely weak in irradiated ices, even though they become readily apparent in the organic residues that result from the warming of the same irradiated ices (Bernstein *et al.*, 1995; Muñoz Caro and Schutte, 2003), and grow when the residues are maintained at room temperature for several hours.

This suggests that the most likely environments in which HMT and its variants might be detected would be those in which astrophysical ices are being sublimed or sputtered away and these molecules are either in organic residues on the surfaces of grains or released into the gas phase. This would include environments such as the clouds in star formation regions and surrounding protostellar objects, in the disks of protoplanetary systems, and perhaps on Saturn's moon Titan.

**4.2.2. Vibrational modes in the IR.** As noted earlier, the IR spectrum of HMT is relatively simple for a molecule of its size, largely because the high symmetry of the molecule

results in a significant number of degenerate vibrational modes (Fig. 4a, b), and only the $T_2$ triply degenerate modes are IR active. The addition of a side group to HMT breaks this symmetry and results in a more complex spectrum because the side group (1) breaks the symmetry of the HMT cage and causes IR inactive modes to become weakly active, (2) breaks the degeneracies in the original HMT cage and causes bands to split, and (3) the side group produces new bands of its own. This increased spectral complexity is apparent for HMT-methanol (compare Fig. 4b, c), but would be expected to happen to a significant degree from the addition of any side group to the original HMT structure.

A few previous studies estimated the rovibrational spectrum of HMT (Jensen, 2002; Khaikin *et al.*, 2014; Pirali *et al.*, 2014). The calculated harmonic frequencies by Pirali *et al.* (2014) using the B97-1//ANO-DZP level of theory for HMT are remarkably close to the observed lines for the non-C–H stretch vibrational bands, given that the DZP quality basis set includes only $s$, $p$, and $d$ functions for the heavy atoms, and only $s$ and $p$ functions for hydrogen. Anharmonicity correction of these vibrational modes is likely to further lower the frequencies by 10–30 cm$^{-1}$, in many cases taking them below the observed fundamental. Vibrational frequencies reported in this work are obtained by using a better ωB97X-D/cc-pVTZ level of theory. Interestingly, it is clear from the low-resolution gas-phase IR absorption spectrum of HMT (Pirali *et al.*, 2014) that the C–H stretch region contains several Fermi resonances similar to PAH molecules (Mackie *et al.*, 2015). One possible Fermi resonance that would need to be considered is combination or overtone bands that include the $A_1$ band at 1556 cm$^{-1}$ and the $T_2$ band at 1532 cm$^{-1}$. Although some experimental and theoretical vibrational analysis has been performed for HMT, there are, however, no such rovibrational data available for other HMT derivatives such as HMT-CH$_2$OH.

It is clear that while the addition of a side group changes the spectrum of the original HMT considerably, it does not greatly affect some of the stronger bands seen in the spectrum of pure HMT. In particular, the strongest bands produced by HMT near 1299 and 1063 cm$^{-1}$ (7.698 and 9.407 μm, respectively), both associated with antisymmetric C–N stretching modes, do not change greatly in position or relative strengths in the spectrum of HMT-methanol. This is largely because these are due to vibrations with large IR intensities that are associated with the main cage structure of the HMT skeleton, which is similar for both HMT and HMT-methanol. The same is probably true for other HMT variants that contain other side groups (*e.g.*, OH, CH$_3$, or NH$_2$). To a lesser degree, the same is true for the strong C–H stretching vibrations of HMT and HMT-methanol in the 3150–3000 cm$^{-1}$ (3.175–3.333 μm) range, although the spectra differ somewhat more because the HMT-methanol contains a unique –CH$_2$– moiety in the CH$_2$OH side group in addition to the multiple –CH$_2$– moieties in the HMT skeleton.

This spectral behavior may offer some opportunities to search for HMT and related molecular species in space in grain mantles. Indeed, while the family of HMT molecules is expected to be nowhere near as abundant in dense clouds as major ice components such as H$_2$O, CO, and CH$_3$OH, our laboratory work suggests that HMT and its variants are some of the most abundant grain mantle products formed when such ices are irradiated and warmed. Furthermore, since the structural nature of HMT and its variants results in some of these molecules' strongest IR bands falling at nearly the

same spectral positions, the overall absorption in these bands will be stronger than those produced by any single variant. It may therefore be possible to detect the overall family of HMT-related compounds by searching for the family's characteristic strong bands near 1299 cm$^{-1}$ (7.698 μm) and 1063 cm$^{-1}$ (9.407 μm). The latter band falls within the profile of the "10 μm silicate" band. However, should these two features be detected in the correct relative proportions, this would be strong evidence supporting the presence of this family of molecules in space. Establishing which members of the overall family are present would be a far more difficult challenge, as it would require the detection of weaker bands specific to individual family members, but could be performed, at least in principle.

HMT bands are among the strongest seen in the IR spectra of the residues formed from the irradiation of astrophysical ice analogues containing H$_2$O, CH$_3$OH, and NH$_3$ (Bernstein *et al.*, 1995; Muñoz Caro and Schutte, 2003; Muñoz Caro *et al.*, 2004). This is both because HMT and its variants are major products of the ice irradiation and warm-up process and because the strongest vibrational modes of the HMT cage have very strong intrinsic strengths (Tables 2 and 3). Nonetheless, the detection of HMT-related bands may be difficult in space because of spectral confusion and because the absolute abundances of these molecules are expected to be modest compared with the dominant ice components. Bernstein *et al.* (1995) demonstrated that UV irradiation and warm-up of an H$_2$O:CH$_3$OH:CO:NH$_3$ = 100:50:10:10 ice resulted in the conversion of ∼40% of the nitrogen from NH$_3$ and 10% of the carbon from CH$_3$OH into HMT. In their experiment, a mixed molecular ice with an H$_2$O column density of $3.6 \times 10^{19}$ molecules cm$^{-2}$ resulted in a column density of HMT of $3.8 \times 10^{17}$ molecules cm$^{-2}$, that is, slightly more than 1% of the original ice's column density. Thus, given that the strongest HMT-related IR bands have high intrinsic strengths and provide good spectral contrast (the lines are relatively narrow in the solid state; ∼15–30 cm$^{-1}$), they may well be detectible as weak IR absorption bands in the right environments. Nonetheless, some bands, such as the C–H stretching modes, occur in many other molecules that might be expected to be present, such as PAH molecules, so one would need to identify multiple bands that have the correct approximate relative intensities to constrain the presence of either HMT or HMT-CH$_2$OH. In this regard, the relative intensities of the C–N single bond stretching modes that occur near 1050 and 1300 cm$^{-1}$ and the HCO bending modes would provide the best tests (see Tables 2 and 3 and the discussion near the end of Section 3).

4.2.3. *Rotational transitions at longer wavelengths.* HMT is a spherical top molecule with a rotational constant $B$ of 0.06306 cm$^{-1}$ (1.89050 GHz), but its high degree of symmetry results in the molecule having no dipole moment, so it is not expected to produce observable rotational bands. It has been noted that deuteration of HMT would break the tetrahedral symmetry of the original molecule, and it would then be detectable using microwave spectroscopy (Oba *et al.*, 2017), although the transitions would be very weak. This is simply due to the fact that the nonzero dipole moment would be due entirely to vibrational averaging effects and thus the permanent dipole moment would be very small, probably less than 0.1 D. For example, the permanent dipole moments for deuterated versions of methane and benzene

are much less than 0.1 D (Hollenstein *et al.*, 1994; Arapiraca and Mohallem, 2016). XYZ coordinates of HMT and HMT–methanol, and components of the dipole moment of HMT–methanol are given in appendix table A1.

The addition of side groups to HMT breaks the original tetrahedral symmetry and such variants will be asymmetric top molecules that have nonzero dipole moments that depend on the nature of the side group. In the case of HMT-methanol, the computed rotational constants are 0.06026, 0.02896, and 0.02858 cm$^{-1}$ (1.80647, 0.86828, and 0.85677 GHz, respectively), and the molecule has a significant computed dipole moment of 1.42 D (for comparison, the dipole moment of $H_2O$ is 1.85 D; Lide, 2003). Thus, HMT-methanol would be expected to produce detectable rotational lines that fall in the submillimeter to millimeter spectral range. HMT variants that differ from HMT-methanol by the presence of other possible side groups would be expected to behave similarly. Given the spectral confusion expected for the vibrational modes of HMT and its variants in the IR, rotational transitions would therefore offer the best hope for identifying individual HMT variants.

However, such searches would be difficult for several reasons. First, as noted previously, the vast majority of HMT and its variants produced by ice irradiation and subsequent warm-up end up in refractory organic grain mantles, not in the gas phase. Introduction of these species into the gas phase would require additional processing of these materials. While these species may be relatively abundant in the residues, they will likely be much less abundant in the gas phase.

Second, rotational lines typically need to be accurate to 1 MHz or better to be assigned to an individual molecule. Unfortunately, calculating the exact predicted positions of the rotation lines is difficult for molecules with the large size of HMT and its variants, and because such calculations require a full consideration of anharmonic effects. Such accuracy from computed rotational constants has been achieved for some small molecules (Puzzarini *et al.*, 2010), but not for molecules the size of HMT. Thus, the detection of rotational lines will require laboratory studies and our computational results only provide some indication as to where to search for them in such future laboratory work.

### 4.3. Astrobiological significance

HMT has been detected in all residues produced from the UV irradiation of starting ice mixtures that contained $CH_3OH$ and $NH_3$, species that are present in ices in a wide range of astrophysical environments. The high efficiency of conversion of $NH_3$ into HMT (Bernstein *et al.*, 1995) was even proposed to be an explanation for the observed low abundance of $NH_3$ in these environments (Muñoz Caro and Schutte, 2003). In any case, HMT, its derivatives, and their precursors should be formed in significant abundances in many cold astrophysical environments, including interstellar dense molecular clouds and protostellar disks. Once formed, these materials can survive in the organic coatings on grains, be incorporated into small objects such as asteroids and comets during the formation of new stellar systems, and subsequently be delivered to the surfaces of planets.

HMT is known to degrade into a multitude of organics. The photodegradation of HMT is known to yield species such as formaldehyde, methyl amines, methane, ammonia, oxides of carbon and nitrogen, ethyl acetate, carbodiimides

(RN=C=NR), hydrocarbons, as well as aliphatic and conjugated isonitriles and nitriles (R–N≡C and R–C≡N, respectively) (Bernstein *et al.*, 1994, 1995; Cottin *et al.*, 2002). Thermodegradation of HMT is known to yield methylamines, methane, ammonia, and oxides of carbon and nitrogen (Iwakami *et al.*, 1968). In addition, the acidic hydrolysis of HMT was shown to lead to the formation of smaller organic compounds including several biological amino acids such as glycine, alanine, phenylalanine, serine, valine, leucine, isoleucine, threonine, and aspartic acid (Wolman *et al.*, 1971). Finally, a recent experimental study simulating hydrothermal conditions at 150°C showed that HMT degrades into a multitude of N-bearing organic compounds, which include *N,N*-dimethylformamide and a wide variety of *N*-heterocycles such as pyridine, pyrazine, pyrrole, pyrazole, and imidazole derivatives (Vinogradoff *et al.*, 2018), which are also compounds of biological interest.

The photodegradation, thermodegradation, and hydrolysis products of other HMT derivatives, including HMT-methanol, are not known, mostly because they are not available as commercial standards. However, the degradation processes of HMT derivatives should produce similar products to those from HMT, that is, methylamines, methane, ammonia, oxides of carbon and nitrogen, and a wider range of amino acids. Degradation of HMT-related compounds in objects such as asteroids could then potentially account for some of the wide variety of amino acids (more than 70) and other organic compounds observed in meteorites (Shock and Schulte, 1990; Sephton, 2002), particularly those whose parent bodies experience aqueous alteration. Similar degradation of HMT and its derivatives would also take place on the surface of a planet, particularly one that supports a hydrosphere. Therefore, HMT, its derivatives, and their degradation products may have played a significant role in prebiotic chemistry as precursors of a wide variety of compounds of biological significance. These compounds may have been part of the inventory available to play a role in the emergence of life on Earth.

### 5. Conclusions

Laboratory experiments suggest that HMT-methanol ($C_7N_4H_{14}O$) is likely to be a common product resulting from the radiation processing of astrophysical ice analogues containing simple source molecules consisting of C, H, O, and N atoms. This molecule differs from simple HMT, which is also known to be abundant in similar ice photolysis residues, by the replacement of a peripheral H atom with a $CH_2OH$ group. As with HMT, HMT-methanol is likely to be a precursor to amino acids as well as a multitude of organics of astrobiological and prebiotic interest. HMT-methanol is also expected to produce a characteristic IR spectrum that shares several vibration features with those of HMT and that can potentially be used to detect and identify it in space. Unlike HMT, which is highly symmetric, HMT-methanol should produce rotational transitions that could be observed at longer wavelengths, although establishing the exact positions of these transitions will be challenging.

### Acknowledgment

## Author Disclosure Statement

## Funding Information

## References

Arapiraca, A.F.C. and Mohallem, J.R. (2016) Vibrationally averaged dipole moments of methane and benzene isotopologues. *J Chem Phys* 144:144301.

Ashbourn, S.F.M., Elsila, J.E., Dworkin, J.P., Bernstein, M.P., Sandford, S.A., and Allamandola, L.J. (2007) Ultraviolet photolysis of anthracene in $H_2O$ interstellar ice analogs: potential connection to meteoritic organics. *Meteorit Planet Sci* 42:2035.

Bera, P.P., Nuevo, M., Milam, S.N., Sandford, S.A., and Lee, T.J. (2010) Mechanism for the abiotic synthesis of uracil via UV-induced oxidation of pyrimidine in pure $H_2O$ ices under astrophysical conditions. *J Chem Phys* 133:104303.

Bera, P.P., Nuevo, M., Materese, C.K., Sandford, S.A., and Lee, T.J. (2016) Mechanisms for the formation of thymine under astrophysical conditions and implications for the origin of life. *J Chem Phys* 144:144308.

Bera, P.P., Stein, T., Head-Gordon, M., and Lee, T.J. (2017) Mechanisms of the Formation of adenine, guanine, and their analogues in UV-irradiated mixed $NH_3:H_2O$ molecular ices containing purine. *Astrobiology* 17:771–785.

Bernstein, M.P., Sandford, S.A., Allamandola, L.J., and Chang, S. (1994) Infrared spectrum of matrix-isolated hexamethylenetetramine in Ar and $H_2O$ at cryogenic temperatures. *J Phys Chem* 98:12206–12210.

Bernstein, M.P., Sandford, S.A., Allamandola, L.J., Chang, S., and Scharberg, M.A. (1995) Organic compounds produced by photolysis of realistic interstellar and cometary ice analogs containing methanol. *Astrophys J* 454:327–344.

Bernstein, M.P., Sandford, S.A., Allamandola, L.J., Gillette, J.S., Clemett, S.J., and Zare, R.N. (1999) UV irradiation of polycyclic aromatic hydrocarbons in ices: production of alcohols, quinones, and ethers. *Science* 283:1135–1138.

Bernstein, M.P., Dworkin, J.P., Sandford, S.A., and Allamandola, L.J. (2001) Ultraviolet irradiation of naphthalene in $H_2O$ ice: implications for meteorites and biogenesis. *Meteorit Planet Sci* 36:351–358.

Bernstein, M.P., Dworkin, J.P., Sandford, S.A., Cooper, G.W., and Allamandola, L.J. (2002a) Racemic amino acids from the ultraviolet photolysis of interstellar ice analogues. *Nature* 416:401–403.

Bernstein, M.P., Elsila, J.E., Dworkin, J.P., Sandford, S.A., Allamandola, L.J., and Zare, R.N. (2002b) Side group addition to the polycyclic aromatic hydrocarbon coronene by ultraviolet photolysis in cosmic ice analogs. *Astrophys J* 576:1115–1120.

Bernstein, M.P., Moore, M.H., Elsila, J.E., Sandford, S.A., Allamandola, L.J., and Zare, R.N. (2003) Side group addition to the polycyclic aromatic hydrocarbon coronene by proton irradiation in cosmic ice analogs. *Astrophys J* 582:L25–L29.

Boogert, A.C.A., Gerakines, P.A., and Whittet, D.C.B. (2015) Observations of the icy Universe. *Ann Rev Astron Astrophys* 53:541–581.

Bregman, J.D., Hayward, T.L., and Sloan, G.C. (2000) Discovery of the 11.2 micron polycyclic aromatic hydrocarbon band in absorption toward Monoceros R2 IRS 3. *Astrophys J* 544:L75–L78.

Briggs, R., Ertem, G., Ferris, J.P., Greenberg, J.M., McCain, P.J., and Schutte, W.M. (1992) Comet Halley as an aggregate of interstellar dust and further evidence for the photochemical formation of organics in the interstellar medium. *Orig Life Evol Biosph* 22:287–307.

Brooke, T.Y., Sellgren, K., and Geballe, T.R. (1999) New 3 micron spectra of young stellar objects with $H_2O$ ice bands. *Astrophys J* 517:883–900.

Chen, Y.-J., Chuang, K.-Y., Muñoz Caro, G.M., Nuevo, M., Chu, C.-C., Yih, T.-S., Ip, W.-H., and Wu, C.-Y.R. (2014) Vacuum ultraviolet emission spectrum measurement of a microwave-discharge hydrogen-flow lamp in several configurations: application to photodesorption of CO ice. *Astrophys J* 781:15.

Cheung, A.C., Rank, D.M., Townes, C.H., Thornton, D.D., and Welch, W.J. (1968) Detection of $NH_3$ molecules in the interstellar medium by their microwave emission. *Phys Rev Lett* 21:1701–1705.

Chiar, J.E., Tielens, A.G.G.M., Whittet, D.C.B., Schutte, W.A., Boogert, A.C.A., Lutz, D., van Dishoeck, E.F., and Bernstein, M.P. (2000) The composition and distribution of dust along the line of sight toward the Galactic Center. *Astrophys J* 537:749–762.

Cottin, H., Szopa, C., and Moore, M.H. (2001) Production of hexamethylenetetramine in photolyzed and irradiated interstellar cometary ice analogs. *Astrophys J* 561:L139–L142.

Cottin, H., Bachir, S., Raulin, F., and Gazeau, M.-C. (2002) Photodegradation of hexamethylenetetramine by VUV and its relevance for CN and HCN extended sources in comets. *Adv Space Res* 30:1481–1488.

Dartois, E. (2005) The ice survey opportunity of ISO. *Space Sci Rev* 119:293–310.

de Marcellus, P., Bertrand, M., Nuevo, M., Westall, F., and d'Hendecourt, L. (2011) Prebiotic significance of extraterrestrial ice photochemistry: detection of hydantoin in organic residues. *Astrobiology* 11:847–854.

d'Hendecourt, L., Jourdain de Muizon, M., Dartois, E., Breitfellner, M., Ehrenfreund, P., Benit, J., Boulanger, F., Puget, J.L., and Habing, H.J. (1996) ISO-SWS observations of solid state features towards RAFGL 7009S. *Astron Astrophys* 315:L365–L368.

Dickens, J.E., Irvine, W.M., De Vries, C.H., and Ohishi, M. (1997) Hydrogenation of interstellar molecules: a survey for methylenimine ($CH_2NH$). *Astrophys J* 479:307–312.

Dunning, T.H. (1989) Gaussian basis sets for use in correlated molecular calculations. I. The atoms boron through neon and hydrogen. *J Chem Phys* 90:1007–1023.

Dworkin, J.P., Deamer, D.W., Sandford, S.A., and Allamandola, L.J. (2001) Self-assembling amphiphilic molecules: synthesis in simulated interstellar/precometary ices. *Proc Natl Acad Sci U S A* 98:815–819.

Dworkin, J.P., Gillette, J.S., Bernstein, M.P., Sandford, S.A., Allamandola, L.J., Elsila, J.E., McGlothlin, D.R., and Zare, R.N. (2004) An evolutionary connection between interstellar ices and IDPs? Clues from mass spectroscopy measurements of laboratory simulations. *Adv Space Res* 33:67–71.

Elsila, J.E., Dworkin, J.P., Bernstein, M.P., Martin, M.P., and Sandford, S.A. (2007) Mechanisms of amino acid formation in interstellar ice analogs. *Astrophys J* 660:911–918.

Gerakines, P.A., Moore, M.H., and Hudson, R.L. (2000) Carbonic acid production in $H_2O:CO_2$ ices. *Astron Astrophys* 357:793–800.

Gerakines, P.A., Moore, M.H., and Hudson, R.L. (2001) Energetic processing of laboratory ice analogs: UV photolysis versus ion bombardment. *J Geophys Res* 106:33381–33385.

Gerakines, P.A., Moore, M.H., and Hudson, R.L. (2004) Ultraviolet photolysis and proton irradiation of astrophysical ice analogs containing hydrogen cyanide. *Icarus* 170:202–213.

Gibb, E.L., Whittet, D.C.B., Schutte, W.A., Boogert, A.C.A., Chiar, J.E., Ehrenfreund, P., Gerakines, P.A., Keane, J.V., Tielens, A.G.G.M., van Dishoeck, E.F., and Kerkhof, O. (2000) An inventory of interstellar ices toward the embedded protostar W33A. *Astrophys J* 536:347–356.

Gibb, E.L., Whittet, D.C.B., Boogert, A.C.A., and Tielens, A.G.G.M. (2004) Interstellar ice: the infrared space observatory legacy. *Astrophys J Suppl Ser* 151:35–73.

Godfrey, P.D., Brown, R.D., Robinson, B.J., and Sinclair, M.W. (1973) Discovery of interstellar methanimine (formaldimine). *Astrophys Lett* 13:119–121.

Harich, S., Lin, J.J., Lee, Y.T., and Yang, X. (1999) Competing atomic and molecular hydrogen pathways in the photodissociation of methanol at 157 nm. *J Chem Phys* 111:5–9.

Hollenstein, H., Marquardt, R.R., Quack, M., and Suhm, M.A. (1994) Dipole moment function and equilibrium structure of methane in an analytical, anharmonic nine-dimensional potential surface related to experimental rotational constants and transition moments by quantum Monte Carlo calculations. *J Chem Phys* 101:3588–3602.

Huang, X. and Lee, T.J. (2008) A procedure for computing accurate *ab initio* quartic force fields: application to $HO_2^+$ and $H_2O$. *J Chem Phys* 129:044312.

Iwakami, Y., Takazono, M., and Tsuchiya, T. (1968) Thermal decomposition of hexamethylene tetramine. *Bull Chem Soc Japan* 41:813–817.

Jensen, J.O. (2002) Vibrational frequencies and structural determinations of hexamethylenetetramine. *Spectrochim Acta A* 58:1347–1364.

Joblin, C., d'Hendecourt, L., Léger, A., and Défourneau, D. (1994) Infrared spectroscopy of gas-phase PAH molecules. 1: role of the physical environment. *Astron Astrophys* 281:923–936.

Khaikin, L.S., Grikina, O.E., Kochikov, I.V., and Stepanov, N.F. (2014) Hexamethylenetetramine (urotropine) $C_6H_{12}N_2$: interpreting the vibrational spectra of -$d_0$ and -$d_{12}$ isotopomers by scaling the quantum-chemical force field. *Russ J Phys Chem A* 88:450–456.

Lacy, J.H., Faraji, H., Sandford, S.A., and Allamandola, L.J. (1998) Unraveling the 10 micron ''silicate'' feature of protostars: the detection of frozen interstellar ammonia. *Astrophys J* 501:L105–L109.

Lee, T.J., Martin, J.M.L., and Taylor, P.R. (1995) An accurate *ab initio* quartic force field and vibrational frequencies for $CH_4$ and isotopomers. *J Chem Phys* 102:254–261.

Lide, D.R. (2003) *CRC Handbook of Chemistry and Physics*, 84th ed. CRC Press, Boca Raton, Florida.

Mackie, C.J., Candian, A., Huang, X., Maltseva, E., Petrignani, A., Oomens, J., Buma, W.J., Lee, T.J., and Tielens, A.G.G.M. (2015) The anharmonic quartic force field infrared spectra of three polycyclic aromatic hydrocarbons: naphthalene, anthracene, and tetracene. *J Chem Phys* 143:224314.

Mardirossian, N. and Head-Gordon, M. (2017) Thirty years of density functional theory in computational chemistry: an overview and extensive assessment of 200 density functionals. *Mol Phys* 115:2315–2372.

Materese, C.K., Nuevo, M., Bera, P.P., Lee, T.J., and Sandford, S.A. (2013) Thymine and other prebiotic molecules produced from the ultraviolet photo-irradiation of pyrimidine in simple astrophysical ice analogs. *Astrobiology* 13:948–962.

Materese, C.K., Nuevo, M., and Sandford, S.A. (2017) The formation of nucleobases from the ultraviolet photoirradiation of purine in simple astrophysical ice analogs. *Astrobiology* 17:761–770.

Materese, C.K., Nuevo, M., McDowell, B.L., Buffo, C.E., and Sandford, S.A. (2018) The photochemistry of purine in ice analogs relevant to dense interstellar clouds. *Astrophys J* 864:44.

Mathis, J.S., Mezger, P.G., and Panagia, N. (1983) Interstellar radiation field and dust temperatures in the diffuse interstellar matter and in giant molecular clouds. *Astron Astrophys* 128:212–229.

Meinert, C., Myrgorodska, I., de Marcellus, P., Buhse, T., Nahon, L., Hoffmann, S.V., d'Hendecourt, L., and Meierhenrich, U.J. (2016) Ribose and related sugars from ultraviolet irradiation of interstellar ice analogs. *Science* 352:208–212.

Muñoz Caro, G.M. and Schutte, W.A. (2003) UV-photoprocessing of interstellar ice analogs: new infrared spectroscopic results. *Astron Astrophys* 412:121–132.

Muñoz Caro, G.M., Meierhenrich, U.J., Schutte, W.A., Barbier, B., Arcones Segovia, A., Rosenbauer, H., Thiemann, W.H.-P., Brack, A., and Greenberg, J.M. (2002) Amino acids from ultraviolet irradiation of interstellar ice analogues. *Nature* 416:403–406.

Muñoz Caro, G.M., Meierhenrich, U., Schutte, W.A., Thiemann, W.H.-P., and Greenberg, J.M. (2004) UV-photoprocessing of interstellar ice analogs: detection of hexamethylenetetramine-based species. *Astron Astrophys* 413:209–216.

Nuevo, M., Chen, Y.-J., Yih, T.-S., Ip, W.-H., Fung, H.-S., Cheng, C.-Y., Tsai, H.-R., and Wu, C.-Y.R. (2007) Amino acids formed from the UV/EUV irradiation of inorganic ices of astrophysical interest. *Adv Space Res* 40:1628–1633.

Nuevo, M., Auger, G., Blanot, D., and d'Hendecourt, L. (2008) A detailed study of the amino acids produced from the vacuum UV irradiation of interstellar ice analogs. *Orig Life Evol Biosph* 38:37–56.

Nuevo, M., Milam, S.N., Sandford, S.A., Elsila, J.E., and Dworkin, J.P. (2009) Formation of uracil from the ultraviolet photo-irradiation of pyrimidine in pure $H_2O$ ices. *Astrobiology* 9:683–695.

Nuevo, M., Bredehöft, J.H., Meierhenrich, U.J., d'Hendecourt, L., and Thiemann, W.H.-P. (2010) Urea, glycolic acid, and glycerol in an organic residue produced by ultraviolet irradiation of interstellar/pre-cometary ice analogs. *Astrobiology* 10:245–256.

Nuevo, M., Milam, S.N., and Sandford, S.A. (2012) Nucleobases and prebiotic molecules in organic residues produced from the ultraviolet photo-irradiation of pyrimidine in $NH_3$ and $H_2O+NH_3$ ices. *Astrobiology* 12:295–314.

Nuevo, M., Materese, C.K., and Sandford, S.A. (2014) The photochemistry of pyrimidine in realistic astrophysical ices and the production of nucleobases. *Astrophys J* 793:125.

Nuevo, M., Sandford, S.A., Materese, C.K., and Cooper, G.W. (2015) Search for sugars and related compounds in residues produced from the UV irradiation of astrophysical ice analogs [abstract PHYS 272]. In *American Chemical Society Fall Meeting*, August 16–20, 2015, Boston, MA.

Nuevo, M., Cooper, G., and Sandford, S.A. (2018) Deoxyribose and deoxysugar derivatives from photoprocessed astrophysical ice analogues and comparison to meteorites. *Nat Commun* 9:5276.

Oba, Y., Takano, Y., Naraoka, H., Kouchi, A., and Watanabe, N. (2017) Deuterium fractionation upon the formation of hexamethylenetetramines through photochemical reactions of interstellar ice analogs containing deuterated methanol isotopologues. *Astrophys J* 849:122.

Öberg, K.I., Garrod, R.T., van Dishoeck, E.F., and Linnartz, H. (2009) Formation rates of complex organics in UV irradiated $CH_3OH$-rich ices. *Astron Astrophys* 504:891–913.

Pirali, O., Boudon, V., Carrasco, N., and Dartois, E. (2014) Rotationally resolved IR spectroscopy of hexamethylenetetramine (HMT) $C_6N_4H_{12}$. *Astron Astrophys* 561:A109.

Prasad, S.S. and Tarafdar, S.P. (1983) UV radiation field inside dense clouds: its possible existence and chemical implications. *Astrophys J* 267:603–609.

Puzzarini, C., Stanton, J., and Gauss, J. (2010) Quantum-chemical calculation of spectroscopic parameters for rotational spectroscopy. *Int Rev Phys Chem* 29:273–367.

Riffet, V., Frisson, G., and Bouchoux, G. (2018) Quantum-chemical modeling of the first steps of the Strecker synthesis: from the gas-phase to water solvation. *J Phys Chem A* 122:1643–1657.

Sandford, S.A., Bera, P.P., Lee, T.J., Materese, C.K., and Nuevo, M. (2015) Photosynthesis and photo-stability of nucleic acids in prebiotic extraterrestrial environments. In *Photoinduced Phenomena in Nucleic Acids II*, Topics in Current Chemistry, Vol. 356, edited by M. Barbatti, A.C. Borin, and S. Ullrich, Springer-Verlag, Berlin, Heidelberg, pp 123–164.

Sellgren, K., Brooke, T.Y., Smith, R.G., and Geballe, T.R. (1995) A new 3.25 micron absorption feature toward Monoceros R2/IRS 3. *Astrophys J* 449:L69–L72.

Sephton, M.A. (2002) Organic compounds in carbonaceous meteorites. *Nat Prod Rep* 19:292–311.

Shao, Y., Gan, Z., Epifanovsky, E., Gilbert, A.T.B., Wormit, M., Kussmann, J., Lange, A.W., Behn, A., Deng, J., Feng, X., Ghosh, D., Goldey, M., Horn, P.R., Jacobson, L.D., Kaliman, I., Khaliullin, R.Z., Kuś, T., Landau, A., Liu, J., Proynov, E.I., Rhee, Y.M., Richard, R.M., Rohrdanz, M.A., Steele, R.P., Sundstrom, E.J., Woodcock, H.L., III, Zimmerman, P.M., Zuev, D., Albrecht, B., Alguire, E., Austin, B., Beran, G.J.O., Bernard, Y.A., Berquist, E., Brandhorst, K., Bravaya, K.B., Brown, S.T., Casanova, D., Chang, C.-M., Chen, Y., Chien, S.H., Closser, K.D., Crittenden, D.L., Diedenhofen, M., DiStasio, R.A., Jr., Do, H., Dutoi, A.D., Edgar, R.G., Fatehi, S., Fusti-Molnar, L., Ghysels, A., Golubeva-Zadorozhnaya, A., Gomes, J., Hanson-Heine, M.W.D., Harbach, P.H.P., Hauser, A.W., Hohenstein, E.G., Holden, Z.C., Jagau, T.C., Ji, H., Kaduk, B., Khistyaev, K., Kim, J., Kim, J., King, R.A., Klunzinger, P., Kosenkov, D., Kowalczyk, T., Krauter, C.M., Lao, K.U., Laurent, A.D., Lawler, K.V., Levchenko, S.V., Lin, C.Y., Liu, F., Livshits, E., Lochan, R.C., Luenser, A., Manohar, P., Manzer, S.F., Mao, S.-P., Mardirossian, N., Marenich, A.V., Maurer, S.A., Mayhall, N.J., Neuscamman, E., Oana, C.M., Olivares-Amaya, R., O'Neill, D.P., Parkhill, J.A., Perrine, T.M., Peverati, R., Prociuk, A., Rehn, D.R., Rosta, E., Russ, N.J., Sharada, S.M., Sharma, S., Small, D.W., Sodt, A., Stein, T., Stück, D., Su, Y.-C., Thom, A.J.W., Tsuchimochi, T., Vanovschi, V., Vogt, L., Vydrov, O., Wang, T., Watson, M.A., Wenzel, J., White, A., Williams, C.F., Yang, J., Yeganeh, S., Yost, S.R., You, Z.-Q., Zhang, I.Y., Zhang, X., Zhao, Y., Brooks, B.R., Chan, G.K.L., Chipman, D.M., Cramer, C.J., Goddard, W.A., III, Gordon, M.S., Hehre, W.J., Klamt, A., Schaefer, H.F., III, Schmidt, M.W., Sherrill, C.D., Truhlar, D.G., Warshel, A., Xu, X., Aspuru-Guzik, A., Baer, R., Bell, A.T., Besley, N.A., Chai, J.-D., Dreuw, A., Dunietz, B.D., Furlani, T.R., Gwaltney, S.R., Hsu, C.-P., Jung, Y., Kong, J., Lambrecht, D.S., Liang, W.Z., Ochsenfeld, C., Rassolov, V.A., Slipchenko, L.V., Subotnik, J.E., Van Voorhis, T., Herbert, J.M., Krylov, A.I., Gill, P.M.W., and Head-Gordon, M. (2015) Advances in molecular quantum chemistry contained in the Q-Chem 4 program package. *Mol Phys* 113:184–215.

Shen, C.J., Greenberg, J.M., Schutte, W.A., and van Dishoeck, E.F. (2004) Cosmic ray induced explosive chemical desorption in dense clouds. *Astron Astrophys* 415:203–215.

Shock, E.L. and Schulte, M.D. (1990) Summary and implications of reported amino acid concentrations in the Murchison meteorite. *Geochim Cosmochim Acta* 54:3159–3173.

Simandiras, E.D., Amos, R.D., Handy, N.C., Lee, T.J., Rice, J.E., Reminton, R.B., and Schaefer, H.F., III. (1988) Second-order perturbation theory and configuration interaction theory applied to medium-sized molecules: cyclopropane, ethylenimine, ethylene oxide, fluoroethane, and acetaldehyde. *J Am Chem Soc* 110:1388–1393.

Smith, R.G., Sellgren, K., and Tokunaga, A.T. (1989) Absorption features in the 3 micron spectra of protostars. *Astrophys J* 344:413–426.

Smolin, E.M. and Rapoport, L. (1959) *The Chemistry of Heterocyclic Compounds, s-Triazines and Derivatives*. Interscience, New York, p 26.

Snyder, L.E., Buhl, D., Zuckerman, B., and Palmer, P. (1969) Microwave detection of interstellar formaldehyde. *Phys Rev Lett* 22:679–681.

Vinogradoff, V., Duvernay, F., Danger, G., Theulé, P., and Chiavassa, T. (2011) New insight into the formation of hexamethylenetetramine (HMT) in interstellar and cometary ice analogs. *Astron Astrophys* 530:A128.

Vinogradoff, V., Rimola, A., Duvernay, F., Danger, G., Theulé, P., and Chiavassa, T. (2012) The mechanism of hexamethylenetetramine (HMT) formation in the solid state at low temperature. *Phys Chem Chem Phys* 14:12309–12320.

Vinogradoff, V., Fray, N., Duvernay, F., Briani, G., Danger, G., Cottin, H., Theulé, P., and Chiavassa, T. (2013) Importance of thermal reactivity for hexamethylenetetramine formation from simulated interstellar ices. *Astron Astrophys* 551:A128.

Vinogradoff, V., Bernard, S., Le Guillou, C., and Remusat, L. (2018) Evolution of interstellar organic compounds under asteroidal hydrothermal conditions. *Icarus* 305:358–370.

Warnek, P. (1962) A microwave-powered hydrogen lamp for vacuum ultraviolet photochemical research. *Appl Opt* 1:721–726.

Whittet, D.C.B., Schutte, W.A., Tielens, A.G.G.M., Boogert, A.C.A., de Graauw, T., Ehrenfreund, P., Gerakines, P.A., Helmich, F.P., Prusti, T., and van Dishoeck, E.F. (1996) An ISO SWS view of interstellar ices: first results. *Astron Astrophys* 315:L357–L360.

Wolman, Y., Miller, S. L., Ibanez, J., and Oró, J. (1971) Formaldehyde and ammonia as precursors to prebiotic amino acids. *Science* 174:1039.

Woon, D.E. (2001) Ab initio quantum chemical studies of reactions in astrophysical ices 3. Reactions of $HOCH_2NH_2$ formed in $H_2CO/NH_3/H_2O$ Ices. *J Phys Chem A* 105:9478–9481.

Zeffiro, A., Lazzaroni, S., Merli, D., Profumo, A., Buttafava, A., Serpone, N., and Dondi, D. (2016) Formation of hexamethylenetetramine (HMT) from HCHO and NH₃—relevance to prebiotic chemistry and B3LYP consideration. *Orig Life Evol Biosph* 46:223–231.

Address correspondence to:
*Christopher K. Materese*
*NASA Goddard Space Flight Center*
*Code 691*
*Greenbelt, MD 20771*

*E-mail:* christopher.k.materese@nasa.gov

---

**Abbreviations Used**

BSTFA = *N,O*-bis(trimethylsilyl)trifluoroacetamide
cc-pVTZ = correlation-consistent polarized valence triple-zeta
GC-MS = gas chromatography coupled with mass spectrometry
HMT = hexamethylenetetramine
IR = infrared
ISM = interstellar medium
PAHs = polycyclic aromatic hydrocarbons
SIC = single-ion chromatogram
TIC = total ion chromatogram
TMS = trimethylsylil
UV = ultraviolet

---

# Appendix Table A1

APPENDIX TABLE A1. *XYZ* COORDINATES FOR THE ATOMS IN HEXAMETHYLENETETRAMINE AND HEXAMETHYLENETETRAMINE-METHANOL

*Atomic XYZ coordinates (in Å) of HMT using ωB97X-D/cc-pVTZ*

| | | | |
|---|---|---|---|
| N | −0.8609275496 | 0.8609275496 | 0.8609275496 |
| C | 0.0000000000 | 0.0000000000 | 1.6758421771 |
| H | −0.6257310981 | −0.6257310981 | 2.3140491795 |
| H | 0.6257310981 | 0.6257310981 | 2.3140491795 |
| N | 0.8609275496 | −0.8609275496 | 0.8609275496 |
| C | 1.6758421771 | 0.0000000000 | 0.0000000000 |
| H | 2.3140491795 | −0.6257310981 | −0.6257310981 |
| H | 2.3140491795 | 0.6257310981 | 0.6257310981 |
| N | 0.8609275496 | 0.8609275496 | −0.8609275496 |
| C | 0.0000000000 | 1.6758421771 | 0.0000000000 |
| H | −0.6257310981 | 2.3140491795 | −0.6257310981 |
| H | 0.6257310981 | 2.3140491795 | 0.6257310981 |
| C | −1.6758421771 | 0.0000000000 | 0.0000000000 |
| H | −2.3140491795 | 0.6257310981 | −0.6257310981 |
| H | −2.3140491795 | −0.6257310981 | 0.6257310981 |
| N | −0.8609275496 | −0.8609275496 | −0.8609275496 |
| C | 0.0000000000 | −1.6758421771 | 0.0000000000 |
| H | 0.6257310981 | −2.3140491795 | −0.6257310981 |
| H | −0.6257310981 | −2.3140491795 | 0.6257310981 |
| C | 0.0000000000 | 0.0000000000 | −1.6758421771 |
| H | −0.6257310981 | 0.6257310981 | −2.3140491795 |
| H | 0.6257310981 | −0.6257310981 | −2.3140491795 |

*Atomic XYZ coordinates (in Å) of HMT-methanol using ωB97X-D/cc-pVTZ*

| | | | |
|---|---|---|---|
| N | −1.7300574324 | 0.7205222670 | −0.6962820891 |
| C | −1.0786395433 | −0.2411711650 | −1.5878757001 |

*(continued)*

APPENDIX TABLE A1. (CONTINUED)

*Atomic XYZ coordinates (in Å) of HMT-methanol using ωB97X-D/cc-pVTZ*

| | | | |
|---|---|---|---|
| N | 0.0300806987 | −0.9478189767 | −0.9373741225 |
| H | −1.8179887085 | −0.9727323206 | −1.9179670461 |
| H | −0.6964048082 | 0.2836520438 | −2.4642513873 |
| C | 0.9988837212 | 0.0729222860 | −0.5013808579 |
| N | 0.3954395903 | 1.0061744086 | 0.4613552193 |
| C | 2.3038030665 | −0.5455506370 | −0.0272290472 |
| H | 1.2647110963 | 0.6598627045 | −1.3839884070 |
| C | −0.7166969818 | 1.6696889053 | −0.2248373428 |
| H | −1.1874508446 | 2.3755160866 | 0.4610323764 |
| H | −0.3256529482 | 2.2256639997 | −1.0778029419 |
| C | −2.2301043850 | −0.0170974531 | 0.4657570067 |
| C | −0.5171605173 | −1.6396515225 | 0.2353918401 |
| N | −1.1628020081 | −0.7239179629 | 1.1773813224 |
| H | −1.2498124133 | −2.3733393811 | −0.1042434623 |
| H | 0.2794376570 | −2.1764965501 | 0.7499490749 |
| C | −0.1659949694 | 0.2663940402 | 1.5932382146 |
| H | −2.7115629115 | 0.6815160208 | 1.1518617372 |
| H | −2.9758482614 | −0.7420251479 | 0.1352875244 |
| H | −0.6358935333 | 0.9784344370 | 2.2731276713 |
| H | 0.6299745974 | −0.2376034675 | 2.1393423755 |
| O | 3.2830191319 | 0.4701360403 | −0.0295770856 |
| H | 4.0933329657 | 0.1143333656 | 0.3318780417 |
| H | 2.5483723940 | −1.3462811991 | −0.7325293315 |
| H | 2.2083947838 | −0.9917754549 | 0.9671301264 |

*Dipole moment*

| | | |
|---|---|---|
| 0.4606 | −1.2468 | 0.5026 |

cc-pVTZ, correlation-consistent polarized triple-zeta; HMT, hexamethylenetetramine.